Zeptomole Voltammetric Detection and Electron-Transfer Rate Measurements Using Platinum Electrodes of Nanometer Dimensions

ARTICLE *in* ANALYTICAL CHEMISTRY · SEPTEMBER 2003

Impact Factor: 5.64 · DOI: 10.1021/ac0342931 · Source: PubMed

6 AUTHORS, INCLUDING:

Jingyuan Chen
University of Fukui

107 PUBLICATIONS **941** CITATIONS

SEE PROFILE

Anal. Chem. **2003,** *75,* 3962−3971

Zeptomole Voltammetric Detection and Electron-Transfer Rate Measurements Using Platinum Electrodes of Nanometer Dimensions

John J. Watkins, Jinyuan Chen,† and Henry S. White*

Department of Chemistry, University of Utah, 315 South 1400 East, Salt Lake City, Utah 84112

Héctor D. Abruña

Department of Chemistry & Chemical Biology, Baker Laboratory, Cornell University, Ithaca, New York 14853-1301

Emmanuel Maisonhaute and Christian Amatore

Département de Chimie, Ecole Normale Supérieure, UMR CNRS-ENS-UPMC 8640 "PASTEUR", 24 Rue Lhomond, 75231 Paris Cedex 05, France

The characterization of quasi-hemispherical Pt electrodes of nanometer dimensions (radius 2−150 nm), prepared by electrophoretic coating of etched Pt wires with poly(acrylic acid), is described. The goals of these experiments are to estimate the accuracy of using steady-state voltammetric limiting currents (i_{lim}) in determining the true electrode area and to develop new electrochemical methods for rapidly screening individual electrodes for nonideal geometries. Electrochemical active areas were determined by measuring the electrical charge (Q) associated with oxidation of adsorbed bis(2,2′-bipyridine)chloro(4,4′-trimethylenedipyridine)osmium(II) in fast-scan voltammetric measurements (scan rate 1000 V/s). Voltammetric peaks corresponding to oxidation of as few as ∼7000 molecules (∼11 zmol) at individual electrodes are reported, allowing precise measurement of electrode areas as small as $\sim 10^{-10}$ cm^2. A plot of i_{lim} (for a soluble redox species) versus $Q^{1/2}$ (for an adsorbed redox species), constructed from $i_{lim}-Q^{1/2}$ data pairs obtained as a function of the electrode radius, is shown to be linear if the electrode geometry is independent of electrode radius; departure of experimental values from the straight-line plot is a diagnostic indicator of a nonideal electrode geometry. The results indicate that ∼50% of the electrodes prepared by the electrophoretic polymer-coating procedure are quasi-hemispherical, the remaining being recessed slightly below the polymer coating. The heterogeneous electron-transfer rate constant for the oxidation of the ferrocenylmethyltrimethylammonium cation in H_2O/0.2 M KCl was also determined from steady-state voltammetry using the method of Mirkin and Bard and found to be 4.8 ± 3.2 cm/s with $\alpha = 0.64 \pm 0.15$.

Electrochemical investigations using metal electrodes of nanometer dimensions are primarily motivated by a fundamental interest in electron-transfer kinetics and mass-transport mechanisms within nanoscale domains,[1−3] as well as by analytical applications of small electrodes as probes in scanning microscopies, e.g., scanning tunneling microscopy (STM)[4,5] and scanning electrochemical microscopy (SECM).[6] Electrode size dictates both the temporal and spatial scales of an electrochemical measurement. Thus, metal electrodes with characteristic dimensions approaching 10 nm or less have been reported by several laboratories during the past 15 years[1,4,7] and applied in a wide range of studies, including investigations of the influence of the electrical double layer on molecular transport[8,9] and kinetics,[10] measurement of fast electron-transfer rates not accessible using larger electrodes,[11] single-molecule detection,[12] and high-resolution electrochemical imaging.[13−17]

A key obstacle in the continued development of nanoscale electrodes is the difficulty in fabricating electrodes of well-defined

* Corresponding author: (e-mail) white@chemistry.utah.edu; (tel) 801/585-6256.

† Present address: Department of Applied Physics, Fukui University, 3-9-1 Bunkyo, Fukuishi, 910-8507 Japan.

(1) Morris, R. B.; Franta, D. J.; White, H. S. *J. Phys. Chem.* **1987**, *91*, 3559−3564.
(2) Norton, J. D.; White, H. S.; Feldberg, S. W. *J. Phys. Chem.* **1990**, *94*, 6772−6780.
(3) Smith, C. P.; White, H. S. *Anal. Chem.* **1993**, *65*, 3343−3353.
(4) Penner, R. M.; Heben, M. J.; Lewis, N. S. *Anal. Chem.* **1989**, *61*, 1630−1636.
(5) Bach, C. E.; Nichols, R. J.; Beckmann, W.; Meyer, H.; Shulte, A.; Besenhard, J. O.; Jannakoudakis, P. D. *J. Electrochem. Soc.* **1993**, *140*, 1281−1284.
(6) Mirkin, M. V.; Fan, F.-R. F.; Bard, A. J. *J. Electroanal. Chem.* **1992**, *328*, 47−62.
(7) Pendley, B. D.; Abruna, H. D. *Anal. Chem.* **1990**, *62*, 782−784.
(8) Conyers, J. L.; White, H. S. *Anal. Chem.* **2000**, *72*, 4441−4446.
(9) Chen, S.; Kucernak, A. *Electrochem. Commun.* **2002**, 80−85.
(10) Chen, S.; Kucernak, A. *J. Phys. Chem. B* **2002**, *106*, 9396−9404.
(11) Penner, R. M.; Heben, M. J.; Longin, T. L.; Lewis, N. S. *Science* **1990**, *250*, 1118−1121.
(12) Fan, F. R. F.; Bard, A. J. *Science* **1995**, *267*, 871−874.
(13) Mirkin, M. V. *Anal. Chem.* **1996**, *68*, 177A−182A.
(14) Shao, Y.; Mirkin, M. V.; Fish, G.; Kokotov, S.; Palanker, D.; Lewis, A. *Anal. Chem.* **1997**, *69*, 1627−1634.
(15) Slevin, C. J.; Gray, N. J.; MacPherson, J. V.; Webb, M. A.; Unwin, P. R. *Electrochem. Commun.* **1999**, *1*, 282−288.
(16) Gardener, C. E.; Macpherson, J. V. *Anal. Chem.* **2002**, *74*, 576A-584A.

10.1021/ac0342931 CCC: $25.00
Published on Web 07/19/2003

geometry, by a straightforward and reproducible means, whose size and shape can be readily characterized. Two promising methods recently reported by other laboratories for making electrodes of nanometer dimensions are based on the electrophoretic coating of sharpened metal wires (Pt,[15] Ag[18]) to produce cone or hemispherical electrodes and the drawing of glass-encased Pt wires, using a pipet puller, to produce disk-shaped Pt electodes.[14,19] Both methods yield electrodes with dimensions as small as a few nanometers, but only electrodes of dimensions of >50 nm have been directly evaluated by scanning electron microscopy.[19] Electrode size is generally obtained by the measurement of the steady-state limiting currents corresponding to oxidation or reduction of a dissolved redox species, although this method requires assumption of electrode geometry. Mirkin et al. have shown that steady-state approach curves measured in SECM experiments are sensitive to the electrode shape and thus can be used to evaluate electrode geometry.[6,14]

In the present report, we describe the synthesis and characterization of hemispherical Pt electrodes using a slightly modified version of the electrophoretic coating method reported by Unwin and co-workers.[15] As reported previously, the steady-state voltammetric response of these electrodes is nearly ideal. The electrochemically active areas of these electrodes are determined by measuring the electrical charge associated with oxidation of a known quantity of a redox-active molecule, bis(2,2′-bipyridine)-chloro(4,4′-trimethylenedipyridine)osmium(II), *adsorbed* at the electrode/electrolyte interface. As few as ∼7000 adsorbed redox molecules can be detected by fast-scan cyclic voltammetry, providing a means to measure electrochemically active areas as small as $\sim 10^{-10}$ cm^2. Values of electrode radii obtained by this method are in reasonable agreement with values obtained from steady-state voltammetry, assuming hemispherical electrode geometry for the latter measurements.

The Pt electrodes prepared in this study have also been used to measure the standard heterogeneous rate constant, $k°$, for the ferrocenylmethyltrimethylammonium$^{1+/2+}$ redox system, TMAFc$^{1+/2+}$, in aqueous solutions. The value of $k°$ measured for TMAFc$^{1+/2+}$ in H_2O/0.2 M KCl is found to be similar to that reported for ferrocene$^{0/1+}$ in nonaqueous solutions.

EXPERIMENTAL SECTION

Chemicals. Ferrocenylmethyltrimethylammonium hexafluorophosphate ([TMAFc]PF_6) was prepared by metathesis of the iodide salt (Strem 99%) with ammonium hexafluorophosphate (Strem 99%). The yellow crystals were collected by vacuum filtration and recrystallized from water. [Os(bpy)$_2$(dipy)Cl]PF_6 (bpy = 2,2′-bipyridine; dipy = 4,4′trimethylenedipyridine) was synthesized by literature procedures.[20,21] $NaClO_4$ and KCl (Aldrich) were reagent grade and used as received. All solutions were prepared using 18 MΩ·cm H_2O from a Barnstead E-pure water purification system.

Electrode Fabrication. Inlaid Pt microdisk electrodes were constructed from 25-μm-diameter Pt wire sealed in glass with a hydrogen/oxygen flame. The sealed end was removed with a diamond-coated cutting wheel to expose the Pt microdisk. The electrodes were polished with successively finer grit sandpaper (400-, 600-, and 800-grit Carbimet disks, Buehler) and alumina oxide slurries (0.3- and 0.01-μm diameter) and rinsed with distilled water.

Pt electrodes of nanometer dimensions were constructed using an electrophoretic polymer coating method originally developed by Bach et al. for coating STM tips[5] and adapted by Schulte and Chow for preparing carbon fiber microelectrodes.[22] Slevin et al. demonstrated the use of this method in preparing nanometer-scale Pt electrodes and electrochemical AFM tips,[15] which has been adopted and modified by ourselves[8] and others[10] in previous reports. A Pt microwire (25-μm diameter) is connected to a W rod (FHC, Inc.) with Ag conductive paint (DuPont). The ensemble is then enclosed in a hand-pulled glass capillary such that ∼1 cm of the microwire is protruding. The W rod is secured to the glass capillary for stability with insulating epoxy (Dexter). The glass capillary is then sealed around the Pt microwire by careful heating over a butane flame. The electrode is visually inspected with an optical microscope to ensure that the Pt/W connection is completely enclosed in the capillary. The protruding wire is then trimmed with scissors to a length of 5 mm.

The exposed microwires are electrochemically etched to sharp points in either a 6 M NaCN solution or an ∼50% w/v $CaCl_2$ solution. As reported in the literature, etching in the $CaCl_2$ solution results in a sharp tip with a longer aspect ratio than tips etched in the NaCN solution.[23,24] Both methods result in optically smooth tips with no discernible difference in electrochemical behavior. A vertical translation stage is used to immerse ∼1 mm of the wire in the solution. An ac voltage of ∼5 V is applied between the Pt wire and a large-area carbon electrode. Bubbles are formed at the Pt/solution interface during electrochemical etching; the applied voltage is removed immediately upon cessation of bubbling. After etching, the wires are dipped for ∼1 s in a 3:1 HCl/HNO_3 solution to clean the surface and then thoroughly rinsed in distilled water.

The etched wires are insulated with an electrophoretic paint (PPG, ZQ84-3225) containing polyacrylate (PAA^-). The sharpened wire is completely immersed in a dilute aqueous paint solution (50:1 H_2O/paint) and a dc potential of 1.8 V is applied between the wire and a Pt coil for ∼10 s to oxidize H_2O ($2H_2O \rightarrow O_2 + 4H^+ + 4e^-$) at the Pt wire. PPA^- at the electrode surface is protonated, resulting in the precipitation of an insulating PAAH layer on the electrode. The insulated electrode is removed from solution and dried at 120 °C for 5 min. While drying, the polymer is reported to retract from the sharpened tip of the wire, exposing the electrode surface.[5] To ensure a stable and resilient polymer layer, the electrodes are then treated with UV light (254 nm) for 30 min to photoinduce cross-linking of polymer chains.[25] Coating the wire once results in electrodes with radii in the range 500−1000 nm, as characterized by steady-state voltammetry. The entire coating procedure is repeated to fabricate electrodes with apparent radii of less than 500 nm. Further polymer applications are needed

(17) Macpherson, J. V.; Unwin, P. R. *Anal. Chem.* **2000**, *72*, 276−285.
(18) Gray, N. J.; Unwin, P. R. *Analyst* **2000**, *125*, 889−893.
(19) Katemann, B. B.; Schuhmann, W. *Electroanalysis* **2002**, *14*, 22−28.
(20) Acevedo, D.; Abruna, H. D. *J. Phys. Chem.* **1991**, *95*, 9590−9594.
(21) Buckingham, D. A.; Dwyer, F. P.; Goodwin, H. A.; Sargeson, A. M. *Aust. J. Chem.* **1964**, *17*, 325−336.
(22) Schulte, A.; Chow, R. H. *Anal. Chem.* **1996**, *68*, 3054−3058.
(23) Melmed, A. J. *J. Vac. Sci. Technol. B* **1991**, *9*, 601−608.
(24) Melmed, A. J.; Carroll, J. J. *J. Vac. Sci. Technol. A* **1984**, *2*, 1388−1389.
(25) Stoye, D., Ed. *Paints, Coatings and Solvents*; VCH: Weinheim, Germany, 1993.

to make smaller electrodes; however, it is difficult to precisely predict the electrode size based on the number of polymer applications. Electrodes prepared by this procedure exhibit reproducible voltammetric responses over several days.

Electrochemical Apparatus. A Cypress Systems model EI-400 bipotentiostat interfaced to a PC computer through a National Instruments (NI) data acquisition board (AT-MIO16E−10) was used to collect voltammetric data. Data were recorded using virtual instrumentation written in-house with LabVIEW. A two-compartment, two-electrode cell was employed with the cell and preamplifier enclosed in a Faraday cage. All electrochemical potentials are measured versus a Ag/AgCl reference/counter electrode purchased from Bioanalytical Systems Inc. Fast-scan waveforms (1000 V/s) were recorded with a LeCroy 9410 digital oscilloscope interfaced to a computer through the NI data acquisition board. A NI GPIB instrument driver was modified in-house to control the instrument and transfer the collected waveforms. Fast-scan voltammograms were averaged (200 waveforms) to increase the signal-to-noise ratio. No additional filtering of the data was performed.

RESULTS AND DISCUSSION

Steady-State Voltammetry and Electron Microscopy. The voltammetric response of a Pt electrode corresponding to the oxidation of 2 mM [TMAFc]PF_6 in 0.2 M KCl, and a transmission electron microscopy (TEM) image of the same electrode, are shown in Figure 1. The electrochemical response is nearly ideal, showing little hysteresis on the return scan. The apparent electrochemical radius of the electrode is calculated from the steady-state limiting current, i_{lim}, assuming a hemispherical geometry.

$$i_{lim} = 2\pi nFDC^*r_{app} \quad (1)$$

In eq 1, C^* and D are the bulk concentration (2 mM) and diffusivity (7.5×10^{-6} cm^2/s)[8] of $TMAFc^+$, respectively, r_{app} is the apparent radius, n is the number of electrons transferred per molecule, and F is Faraday's constant. The calculated radius is referred to as an apparent radius in these and prior studies[8] because an ideal hemispherical electrode geometry is assumed. A value of $r_{app} = 70$ nm was computed from the voltammetric response ($i_{lim} = 64$ pA) presented in Figure 1.

Parts b and c of Figure 1 are TEM images (30000× and 100000× magnifications) of the same electrode used to record the voltammetric curve in Figure 1a. The Pt electrode, because of its dense atomic packing, reduces the transmission of the electrons and is manifested as the black protruding hemispheroid. Incident electrons are able to transmit through the edges of the carbon-based polymer, which corresponds to the gray regions of the images. The geometric radius of the electrode in Figure 1, measured from the TEM image, is ~75 nm, in good agreement with the electrochemically measured radius, r_{app}, of 70 nm (Figure 1a).

The TEM images indicate that the electrode geometry is not a true hemisphere embedded in insulating plane of infinite area, as assumed in using eq 1, but is better described as a flattened hemispheroidal electrode, isolated from the solution at the edges by a thin ring of insulating material. The use of eq 1 is

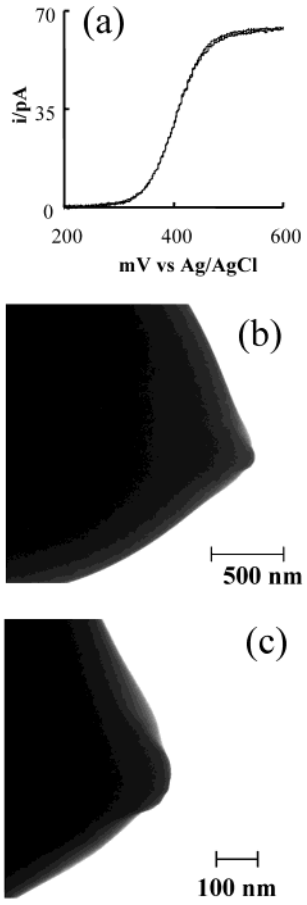

Figure 1. (a) Voltammetric response of a Pt electrode (r_{app} = 70 nm) in an aqueous 2 mM $TMAFc^+$ solution containing 0.2 M KCl as the supporting electrolyte. Scan rate 10 mV/s. TEM images of the same electrode at (b) 30000× and (c) 100000× magnifications. The incident electrons (75 keV) are able to transmit through the edges of insulating polymer (gray regions), but not the Pt electrode. The black protruding hemispheroid is the Pt electrode with $r = 77$ nm.

compromised by both the nonhemispherical geometry and the finite thickness of the insulating sheath. The finite insulating sheath is a concern because it allows the diffusion of molecules to the electrode surface from regions of solution lying along the sides of the wire, potentially resulting in larger currents than predicted by eq 1. We estimated the error that results from use of eq 1 by employing more sophisticated mathematical predictions of the current, found in the literature, for different electrode geometries.[26−28]

Myland and Oldham[27] derived the following analytical equation for the diffusion-limited current to hemispheroidal shaped electrodes embedded in an infinite plane,

$$i_{lim} = 2\pi nFDC^*(r^2 - h^2)^{1/2}/\text{arcosh}(h/r) \quad \text{for} \quad h < r \quad (2)$$

where h is the height of the hemispheroid, r is the radius of the electrode base, and the other terms are as previously defined.[27] The condition $h < r$ corresponds to a flattened hemisphere, which

(26) Fang, Y.; Leddy, J. *Anal. Chem.* **1995**, *67*, 1259−1270.
(27) Myland, J. C.; Oldham, K. B. *J. Electroanal. Chem.* **1990**, *288*, 1−14.
(28) Zoski, C. G.; Mirkin, M. V. *Anal. Chem.* **2002**, *74*, 1986−1992.

best describes the true exposed electrode geometry identified by TEM. From Figure 1, we estimate $h = \sim 35$ nm and compute $i_{lim} = 56$ pA, slightly smaller that the experimental value of 64 pA. The key limitation of eq 2 is that is does not account for diffusion from the backside of the electrode that results from the finite thickness of the insulating sheath. Thus, eq 2 should tend to underestimate value of i_{lim} for our geometry, in agreement with the results.

To account for back-diffusion, we also used the recent numerical simulations of Zoski and Mirkin for the current at a cone-shaped electrode surrounded by a finite insulating sheath.[28] Approximating the height of the cone as $h = 35$ nm and the thickness of the insulating polymer, d, as 100 nm, and employing numerical values tabulated in Table 4 of ref 28, the limiting current for this geometry is given by eq 3,

$$i_{lim} = 4nFDC^*r(1.1270 + (0.1972((d/r) - 0.5667)^{-0.9025} \quad (3)$$

which predicts a value of 59 pA for i_{lim}. Thus, inclusion of the diffusion from the sides of the insulating layer brings the experimental and predicted values into slightly better agreement, but this may be somewhat fortuitous, as the true electrode geometry is clearly too blunt to be described as a finite cone. Of course, it is unlikely that any simple ideal geometry used in mathematical modeling will precisely describe electrodes of nanometer dimensions, as the shapes of the electrodes are difficult to control at these length scales with currently known methods. On the basis of the above comparisons, we conclude that the current is insufficiently sensitive to the precise geometry to allow subtle differences in geometry to be determined by voltammetric measurements.

Determination of Surface Area by Voltammetric Analysis of an Adsorbed Redox-Active Molecule. The preceding section demonstrates that determination of the electrode radius of the nanoscale Pt electrodes from the steady-state voltammetric limiting current, eq 1, is not entirely reliable. In addition, it is not practical to image every individual electrode by TEM to determine the true electrode dimensions and shape. To address this problem, true *electroactive* areas were estimated by measuring the electrical charge associated with the oxidation of a known coverage of a redox-active molecule adsorbed at the Pt surface. In addition to providing a second value of the electrode radius, a comparison of the radius measured by this method with the corresponding value measured using eq 1 provides a quick diagnostic test of nonideal geometries, vide infra. The determination of electrode surface area by measurement of the charge associated with reduction or oxidation of an molecular monolayer or atomic adlayer is frequently employed with macroscopic electrodes.[29]

To measure the area of the Pt electrodes, a monolayer of $[Os(bpy)_2(dipy)Cl]^+$, Figure 2, was adsorbed onto the electrode surface. The electrochemical behavior of adsorbed layers of $[Os(bpy)_2(dipy)Cl]^+$ and related molecules has been extensively studied by Abruña and co-workers,[20,30] who reported that a saturation surface coverage at Pt, Γ^*, corresponds to 1.1×10^{-10} mol/cm^2, independent of surface area.[31] To obtain full monolayer coverage, electrodes were preequilibrated for 30 min in a 0.1 mM solution of $[Os(bpy)_2(dipy)Cl]PF_6$ dissolved in acetone/H_2O (1:10, v/v). The electrode was rinsed thoroughly with deionized water and placed in an O_2-free aqueous 0.2 M $NaClO_4$ solution containing $[Os(bpy)_2(dipy)Cl]PF_6$ at a sufficiently high concentration (3 μM) to maintain a saturated surface coverage at Pt.[20]

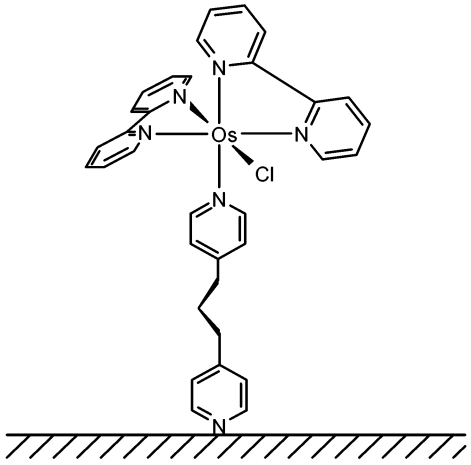

Figure 2. Schematic depiction of the adsorption of $[Os(bpy)_2(dipy)Cl]$ at the Pt/electrolyte interface.

The electrode area, A, is obtained by measuring the electrical charge, Q, associated with the $1 - e^-$ oxidation of the adsorbed $[Os(bpy)_2(dipy)Cl]^+$, eq 4.

$$A = Q/(nF\Gamma^*) \quad (4)$$

The challenge in applying this method to ultrasmall electrodes is that values of Q associated with the adsorbed redox molecules are exceedingly small, making it difficult to measure voltammetric currents above the noise limit of the instrument. The peak voltammetric current for the oxidation (and rereduction) of an adsorbed molecule is given by eq 5,[32]

$$i_p = (n^2F^2/4RT)\nu A\Gamma^* \quad (5)$$

which predicts a voltammetric peak current of 0.0065 pA at $\nu = 0.1$ V/s for the oxidation of a monolayer of $[Os(bpy)_2(dipy)Cl]^+$ at a 100-nm-radius electrode, well below the measured noise level of the instrument at 0.1 V/s ($\pm$2 pA). Thus, significantly faster scan rates are necessary to obtain a measurable signal. For instance, increasing ν to 1000 V/s increases the predicted peak current to 65 pA. However, the instrument noise also increases at higher scan rates ($\pm$160 pA at 1000 V/s). By averaging 200 voltammetric waveforms, a noise level of $\pm$11 pA ($\sim\pm$160 pA/$\sqrt{200}$ waveforms) is obtained, well below the signal from the adsorbed monolayer.

The tradeoff in obtaining larger voltammetric peak currents by increasing ν is that the capacitive current also increases in

(29) Sawyer, D. T.; Roberts, J. *Experimental Electrochemistry for Chemists*; John Wiley and Sons: 1974; pp 74−79.

(30) Hudson, J.; Abruna, H. D. *J. Phys. Chem.* **1996**, *100*, 1036−1042.

(31) The saturation surface coverage of $[Os(bpy)_2(dipy)Cl]^+$ at Pt has been demonstrated to be independent of electrode area between 8.5×10^{-3} and 4.1×10^{-7} cm^2.[20]

(32) Bard, A. J.; Faulkner, L. R. *Electrochemical Methods*, 2nd ed.; John Wiley & Sons: New York, 2001.

proportion to ν. This is a particularly challenging issue with Pt electrodes prepared by electrophoretic coating of Pt wires, as the capacitance per unit area of the electrode/polymer layer/solution interfaces is significant, on the order of 0.2 μF/cm^2 in a 0.2 M KCl solution.[33] While this value is small in comparison to the capacitance per unit area of the exposed Pt/0.2 M KCl interface ($\sim$50 μF/cm^2 [32]), the immersed area of the polymer-coated surface is many orders of magnitude greater than the area of the exposed Pt. For example, the area of a nonelectroactive polymer-coated region of an 100-nm-radius electrode immersed to a depth of 50 μm is 5 orders of magnitude larger than the area of the exposed Pt. Consequently, the capacitive currents in the fast-scan voltammetric currents are dominated by the capacitance of the polymer coating.

To reduce the capacitive current associated with the polymer coating, a thick layer of Apiezon wax was applied to the electrode using a modification of a technique often employed in preparing tips for in situ scanning probe experiments. The electrode is carefully moved horizontally, while rotating, through a molten bead of Apiezon wax supported on a modified soldering iron tip to apply an even coating (see Supporting Information for a schematic drawing of this procedure). The electrode is then placed in an oven for 10 s to allow the wax to retract from the electrode tip.

The steady-state voltammetric response (20 mV/s) of a 170-nm-radius electrode in 2 mM $TMAFc^+$/0.2 M KCl was recorded *before* and *after* applying the Apiezon wax insulation, Figure 3a, to ensure that the application of the Apiezon wax does not modify the electroactive area of the Pt electrode. The limiting current after applying the Apiezon wax increased by a small amount ($\sim$15%), probably due to polymer retraction when the molten wax is applied.

Figure 3b shows the fast-scan voltammetric response ($\nu = 1000$ V/s, average of 200 scans) of the same Pt electrode, before and after coating with Apiezon wax, in a solution containing $[Os(bpy)_2(dipy)Cl]^+$. Prior to coating with Apiezon wax, the capacitive current dominates the overall electrode response, and no voltammetric peak associated with oxidation of $[Os(bpy)_2(dipy)Cl]^+$ is apparent. Applying the Apiezon wax, Figure 3b, reduces the capacitive current by $\sim$1 order of magnitude. Voltammetric waves associated with oxidation and reduction of $[Os(bpy)_2(dipy)Cl]^+$ are clearly discernible in the rescaled voltammetric curves in Figure 3c. The faradaic charge associated with the voltammetric peak ($Q = 3.8 \times 10^{-14}$ C) corresponds to a surface area of 3.6×10^{-9} cm^2, eq 4, corresponding to a hemisphere with a radius of 240 nm. The steady-state limiting current, i_{lim}, corresponds to a hemisphere electrode with an electroactive area equal to 2.5×10^{-9} cm^2. The difference in these values is consistent with oblate hemispheroid electrode geometry.

The voltammetric response of an even smaller Apiezon wax-covered Pt electrode is shown in Figure 4a. From the steady-state limiting current measured in the 2 mM $TMAFc^+$/0.2M KCl solution, r_{app} was determined to be 66 nm for this electrode. The

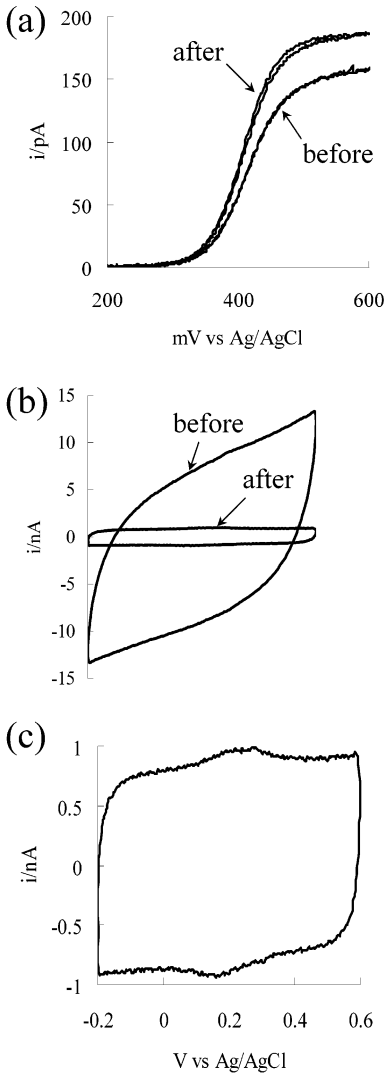

Figure 3. (a) Cyclic voltammogram (20 mV/s) of a Pt electrode ($r_{app} = 170$ nm) in 2 mM $TMAFc^+$/0.2 M KCl, before and after coating with Apiezon wax. (b) Cyclic voltammograms (1000 V/s, 200 waveforms averaged) for the same electrode corresponding to the oxidation and rereduction of adsorbed $[Os(bpy)_2(dipy)Cl]^+$ in 0.2 M $NaClO_4$, before and after Apiezon wax coating. (c) Voltammetric response of the wax-coated electrode from (b) plotted at higher current sensitivity.

voltammetric response of the same electrode for the oxidation of adsorbed $[Os(bpy)_2(dipy)Cl]^+$ at a scan rate of 1000 V/s is shown in Figure 4b. The faradaic current associated with the adsorbed complex is barely visible on the large capacitive current. Figure 4c shows the voltammetric response after removing the majority of the capacitance current and rescaling the currents. For comparison, the solid lines correspond to the theoretical $i-E$ response computed from eq 6,

$$i = \frac{n^2F^2}{RT}\frac{\nu A\Gamma^* \exp[(nF/RT)(E - E^{\circ\prime})]}{\{1 + \exp[(nF/RT)(E - E^{\circ\prime})]\}^2} + \upsilon C_T\left[1 - \exp\left(\frac{-(E - E_i)}{\nu R_s C_T}\right)\right] \quad (6)$$

where the first and second terms on the right-hand side correspond to the faradic and capacitive responses of the electrode.[34]

(33) The electrode/polymer layer/solution capacitance was estimated by recording the voltammetric capacitive current, i_c, of a 12.5-μm-radius polymer-coated wire as a function of the depth of immersion, d, in a 0.2 M KCl solution. The slope of the resulting linear plot of i_c vs d is equal to $(C/A)2\pi r\nu$, where ν is the scan rate (50 V/s), r is the wire radius, and C/A is the capacitance per unit area.

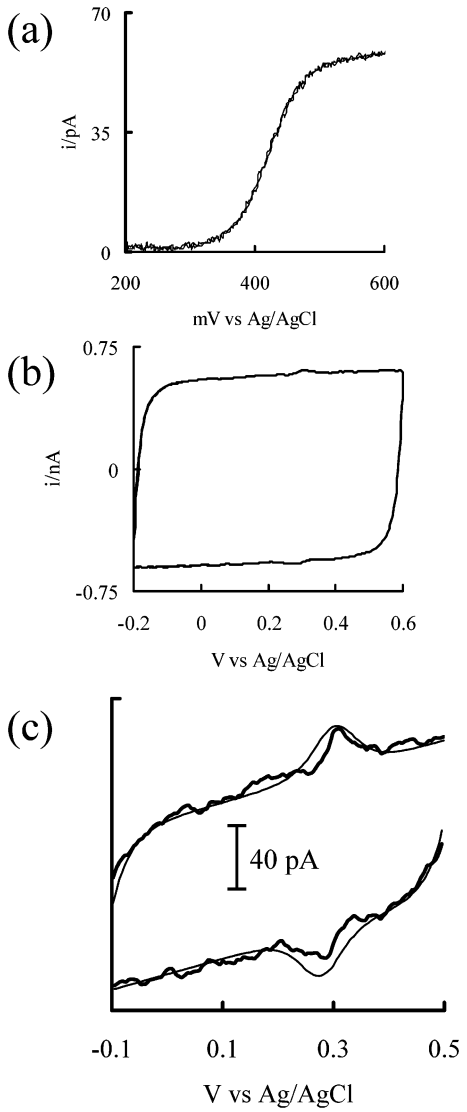

Figure 4. (a) Voltammetric response (10 mV/s) of a Pt electrode (r_{app} = 66 nm) in an aqueous 2 mM $TMAFc^+$/0.2 M KCl solution. (b) Cyclic voltammograms (1000 V/s, 200 waveforms averaged) for the same electrode corresponding to the oxidation and rereduction of adsorbed $[Os(bpy)_2(dipy)Cl]^+$ in 0.2 M $NaClO_4$. (c) Voltammetric response in (b) plotted at higher current sensitivity. The smoothed line is the theoretical prediction based on r_{app} = 66 nm.

In eq 6, R_s is the solution resistance, C_T is the total electrode capacitance (including both insulated and noninsulated regions), $E^{\circ\prime}$ is the formal redox potential of the $[Os(bpy)_2(dipy)Cl]^{+/2+}$ couple, and E_i is the initial potential of the forward and reverse scans. The solid lines were computed using values of $R_s = 47 \times 10^6\ \Omega$, $C_T = 0.57 \times 10^{-12}$ F, and $A = 2\pi r_{app}^2 = 2.74 \times 10^{-10}$ cm^2, where r_{app} is determined from the steady-state response in Figure 4a. Very reasonable agreement between theory and experimental currents is obtained, indicating that the electroactive area is the same in both the steady-state and fast-scan voltammetric measurements. Integration of the voltammetric waves yields an electrical charge (1.1×10^{-15} C) roughly equivalent to 7000 molecules or ~11 zmol. It is clear that the voltammetric peak in Figure 4c is just barely larger than the instrument noise, ~10 pA. Thus, because the area and therefore the current from the adsorbed species decrease rapidly in proportion to the square of the radius, the measurement shown in Figure 4c corresponds roughly to the present limit of detection (S/N ~2).

(34) These terms correspond to eqs 14.3.11 and 1.2.15 in ref 32.

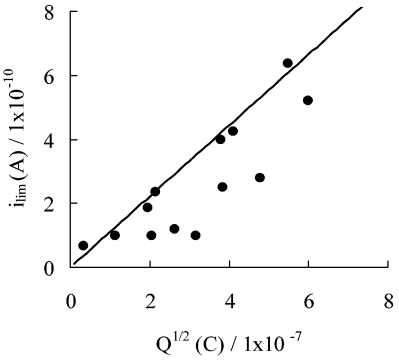

Figure 5. Steady-state limiting voltammetric current, i_{lim}, for the oxidation of $TMAFc^+$ versus the square root of the charge, $Q^{1/2}$, associated with oxidation of adsorbed $[Os(bpy)_2(dipy)Cl]^+$. The solid line is the theoretical curve for ideal electrode geometry and has a slope equal to 1.1×10^{-3} $C^{1/2}$/s (predicted by eq 7).

For any ultramicroelectrode geometry for which a true steady-state voltammetric response is obtained, it is readily shown that the steady-state limiting current, i_{lim}, for the oxidation (or reduction) of a dissolved redox species should vary linearly with the square root of the charge transferred, $Q^{1/2}$, for an adsorbed species. For a hemispherical electrode, this relation is derived by combining eqs 1 and 4.

$$i_{lim} = (2\pi nF/\Gamma^*)^{1/2} DC^* Q^{1/2} \qquad (7)$$

Ideally, for the experiments reported herein, values of i_{lim} (measured for the oxidation of 2 mM $TMAFc^+$) plotted against $Q^{1/2}$ (measured for the oxidation of $[Os(bpy)_2(dipy)Cl]^+$) should yield a straight line with a slope of 1.11×10^{-3} $C^{1/2}$ s ($= (2\pi nF)^{1/2}\Gamma^{*-1/2}DC^*$ for the specific experiments described above). Departure of an $i_{lim}-Q^{1/2}$ datum from this straight line is diagnostic of a nonhemispherical electrode geometry. For instance, if the polymer coating is thick and extends beyond the electrode surface, mass transfer of a solution species is blocked, resulting in currents smaller than those predicted by eq 1, while $Q^{1/2}$ will be largely unaffected. The effects of such a geometry, which have been referred to as lagoon or recessed electrodes, on measurements of electron-transfer rates have been considered by others.[35,36] The $i_{lim}-Q^{1/2}$ datum for such an electrode geometry will lie below the theoretical line. Conversely, increased diffusional transport above that predicted by eq 1, e.g., due to diffusion from the sides of the electrode, will result in an $i_{lim}-Q^{1/2}$ datum lying above the theoretical line. Alternatively, data above the dotted line may also correspond to a Q smaller than expected for a true hemisphere and would be diagnostic of a more planar electrode geometry.

Figure 5 shows a plot of experimental $i_{lim}-Q^{1/2}$ data and the theoretical prediction based on eq 7 for a hemispherical electrode. It is clear that while there is reasonable clustering of the data

(35) Baranski, A. S. *J. Electroanal. Chem.* **1991**, *307*, 287−292.
(36) Oldham, K. B. *Anal. Chem.* **1992**, *64*, 646−651.

about the theoretical line, many values lie below the line suggestive of recessed electrode geometry. For the point lying the largest relative distance away from the theoretical line, the predicted value of i_{lim} is approximately one-fourth the actually observed value. The discrepancy is much smaller for other points that lay off of the line, and as such, we conclude that the majority of the electrodes produced by the electrophoretic coating procedure have a hemispherical or quasi-hemispherical shape. However, kinetic measurements based on measurements using an individual electrode are clearly susceptible to significant error.

Electron-Transfer Rate Constant for $TMAFc^+$ Oxidation. The steady-state voltammetric response of Pt nanoelectrodes, coated with PAAH but not with Apeizon wax, were employed to measure the standard heterogeneous electron-transfer rate constant, $k°$, for $TMAFc^+$ in H_2O. Several efforts in the past decade have focused on measurements of $k°$ for the oxidation of Fc in acetonitrile.[37−39] The interest in the rate constant of this reaction is due, in part, to the fundamental interest in factors that govern the rates of fast outer-sphere reactions (of which the reaction $Fc \rightleftharpoons Fc^+ + e^-$ is a prototypical example) and, in part, to the use of the Fc/Fc^+ couple as a "known" system for comparing the accuracy of different electroanalytical methods used for measuring large rate constants. Measurements by steady-state voltammetry[37] and ac impedance[39] suggest that $k°$ for the Fc/Fc^+ system (in CH_3CN) is ~4 cm/s. While differences in polarization dynamics and electron-transfer distances in different solvents may influence the rate of electron-transfer reactions,[39] simple models of electron transfer suggest that $k°$ for the oxidation of $TMAFc^+$ in H_2O should not be largely different from the values for the oxidation of Fc in CH_3CN.

Measurement of $k°$ requires that the rate of mass transfer of the molecule to the electrode surface be comparable to or greater than the rate of electron transfer. For steady-state voltammetry at a hemispherical electrode, this condition may be expressed as[32,40,41]

$$(D/k°r_{app}) \geq 0.1 \qquad (8)$$

In principle, values of $k°$ between 1 and 100 cm/s can be measured using electrodes with r_{app} between 100 and 1 nm, respectively, assuming a typical value of D (~10^{-5} cm^2/s). Thus, the Pt electrodes described in the previous section appear to be of the appropriate size to determine the rate constant for the oxidation of $TMAFc^+$ in H_2O.

The voltammetric responses of three Pt electrodes with r_{app} of 31.1, 8.8, and 3.2 nm are shown in Figure 6a. Smooth curves are drawn through the raw data and replotted in Figure 6b after normalizing the current to the diffusion-controlled limiting current, i_{lim}, for the purpose of guiding the reader's eye to the dependence of the voltammetric wave shape on r_{app}. In addition, the normalized

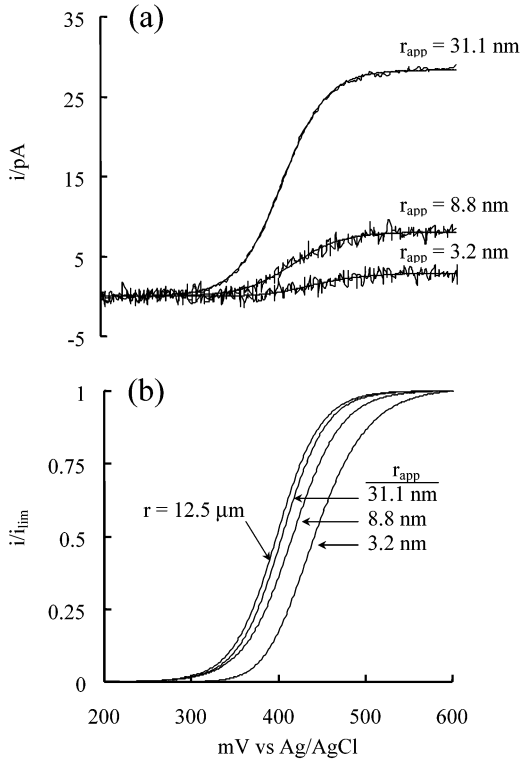

Figure 6. (a) Voltammetric responses of three Pt electrodes (r_{app} = 3.2, 8.8, and 31.1 nm) in an aqueous 2 mM $TMAFc^+$ solution containing 0.2 M KCl. Scan rate 10 mV/s. The smoothed lines drawn through the voltammetric data are replotted in (b) after normalization of the current to the limiting value. For comparison, the normalized voltammetric response of a 25-μm-diameter Pt microdisk electrode in the same solution is also shown.

voltammetric response for $TMAFc^+$ at a 12.5-μm-radius Pt disk is included in the Figure 6b. Examination of the curves indicates that the voltammetric half-wave potential, $E_{1/2}$, shifts toward more positive potentials as r_{app} decreases ($E_{1/2}$ is defined as the potential where the voltammetric current equals half of the diffusion-limited value, i.e., $i = 0.5i_{lim}$).

Our analysis of the voltammetric data in Figure 6 is based on classical Butler−Volmer electrode kinetics, in which the $i-E$ relationship for the oxidation of $TMAFc^+$ can be written as[32,40]

$$i = \frac{nFAC^*k° \exp((1-\alpha)F(E-E°')/RT)}{1 + \frac{r_{app}k°}{D}[\exp(-\alpha F(E-E°')/RT) + \exp((1-\alpha)F(E-E°')/RT)]} \qquad (9)$$

All parameters in eq 9 have been previously defined except for the transfer coefficient, α, and oxidative currents are assigned positive values. In addition, the diffusivities of $TMAFc^+$ and $TMAFc^{2+}$ are assumed to be equal. We have employed the method of Mirkin and Bard[42] for analysis of quasi-reversible steady-state voltammograms to extract values of $k°$ and α from the experimental data. Such an analysis is based on the measurement of experimental parameters ($E_{1/4} - E_{1/2}$) and ($E_{1/2} - E_{3/4}$), where $E_{1/4}$ and $E_{3/4}$ are the quartile potentials, corresponding to the

(37) Mirkin, M. V.; Richards, T. C.; Bard, A. J. *J. Phys. Chem.* **1993**, *97*, 7672−7677.
(38) Wipf, D. O.; Kristensen, E. W.; Deakin, M. R.; Wightman, R. M. *Anal. Chem.* **1988**, *60*, 306−310.
(39) Baranski, A. S.; Winkler, K.; Fawcett, W. R. *J. Electroanal. Chem.* **1991**, *313*, 367−375.
(40) Zoski, C. G. In *Modern Techniques in Electroanalysis*; Vanysek, P., Ed.; Wiley: New York, 1996; pp 241−312.
(41) The condition expressed in eq 8 corresponds to analysis of a 2.5-mV shift in $E_{1/2}$.
(42) Mirkin, M. V.; Bard, A. J. *Anal. Chem.* **1992**, *64*, 2293−2303.

Table 1. Kinetic Parameters for the Oxidation of $TMAFc^+$ at Pt in H_2O/0.2 M KCl

r_{app} (nm)	$\Delta E_{1/4}$ (mV)[a]	$\Delta E_{3/4}$ (mV)[a]	$k°$ (cm/s)[b]	α	$(E_{1/2} - E°')_\Delta$ (mV)[b]	$(E_{1/2} - E°')_{expt}$ (mV)[a]
149.7	29.5	31.0	4.9	0.34	2.6	9.3
113.1	30.0	31.0	3.2	0.59	5.1	10.5
112.6	30.0	31.0	3.2	0.59	5.1	3.8
77.8	31.0	31.5	1.3	0.78	15.4	11.5
73.7	30.0	31.0	4.9	0.59	5.1	8.5
68.5	29.5	31.0	10.9	0.34	2.6	6.2
62.6	30.0	31.0	5.8	0.59	5.1	15.7
48.9	30.0	31.0	7.5	0.59	5.1	7.8
31.7	35.5	36.0	0.6	0.76	48.9	2.0
25.4	32.0	32.5	2.4	0.79	23.5	6.7
22.9	31.5	32.0	3.3	0.79	19.4	4.7
12.0	34.0	34.5	2.5	0.77	38.8	0.9
10.1	34.0	34.5	2.9	0.77	38.8	12.9
8.8	31.5	32.0	8.72	0.79	19.4	18.2
6.1	59.0	60.0	1.4	0.47	116	17.6
3.2	49.0	50.0	3.5	0.55	90.3	43.3
1.8	35.5	36.0	11.7	0.75	90.3	55.4
1.8	49.0	50.0	6.0	0.55	48.9	59.5
1.7	39.6	40.0	6.9	0.69	71.1	39.8
av values			$4.8 \pm 3._2$	$0.6_4 \pm 0.1_5$		

[a] $\Delta E_{1/4}$ ($= E_{1/2} - E_{1/4}$), $\Delta E_{3/4}$ ($= E_{3/4} - E_{1/2}$), and $(E_{1/2} - E°')_{expt}$ are values obtained from the steady-state voltammetric curves recorded at 23 °C. [b] $k°$, α, and $(E_{1/2} - E°')_\Delta$ are predicted from Table 1 of ref 42 based on measured values of $\Delta E_{1/4}$ and $\Delta E_{3/4}$.

electrode potentials where the current is equal to $^1/_4$ and $^3/_4$ of the limiting value, respectively. Experimentally determined values of $(E_{1/4} - E_{1/2})$ and $(E_{1/2} - E_{3/4})$ for individual voltammograms are matched to the corresponding values of $k°$ and α via a numerical look-up table found in ref 41. The reader is referred to ref 42 for details of this straightforward analysis. Values of $k°$ and α, determined by this method for 19 electrodes, with r_{app} ranging from ~2 to ~150 nm, are listed in Table 1. Electrode radii, r_{app}, were calculated from the steady-state limiting currents. Based on this analysis, we determined $k° = 4._8 \pm 3._2$ cm/s and $\alpha = 0.6_4 \pm 0.1_5$.[43]

While considerable scatter exists in the values of $k°$ listed in Table 1, no discernible dependence of $k°$ on r_{app} is evident. This finding is significant and lends validity to the measurement, as the electron-transfer rate should show no dependence on the rate of mass transport to the electrode. For the data in Table 1, the rate of mass transport spans nearly 2 orders of magnitude.

Kinetic analysis of the voltammetric curves was also performed by measuring the dependence of the absolute value of $E_{1/2}$ on r_{app}. Normalizing eq 9 by the expression for the diffusion-limited current (eq 1) and setting i/i_{lim} equal to $^1/_2$, yields the following relationship between $k°$ and experimental $E_{1/2}$ values,

$$k° = (D/r_{app})(\exp((1 - \alpha)F(E_{1/2} - E°')/RT) - \exp(-\alpha F(E_{1/2} - E°')/RT))^{-1} \quad (10)$$

In eq 10, $E°'$ is the formal potential of the $TMAFc^+/TMAFc^{2+}$ redox couple. Assuming equal diffusivities for $TMAFc^+$ and $TMAFc^{2+}$, $E°'$ is equal to $E_{1/2}$ for a reversible voltammetric response. The oxidation of $TMAFc^+$ at the 12.5-μm-radius Pt electrode is expected to be reversible, since $(D/k°r_{app})$ is assumed to be much less than 1 for such a large electrode. This assumption is validated below. Thus, $E_{1/2}$ measured using the 12.5-μm-radius Pt electrode (Figure 6b) can be taken as a good approximation of $E°'$.

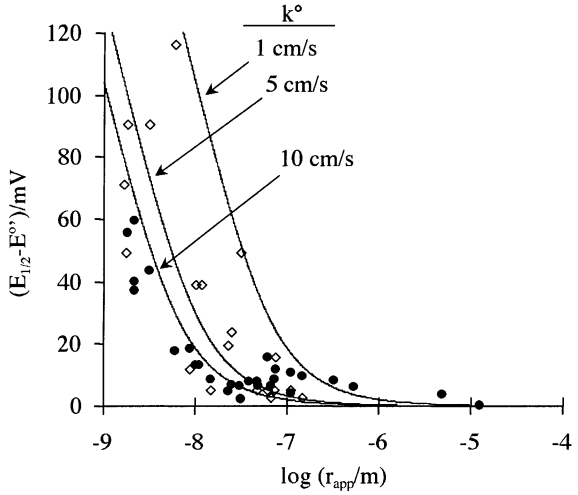

Figure 7. Variation in $(E_{1/2} - E°')$ as a function of r_{app}. The filled circles are measured $(E_{1/2} - E°')_{expt}$ values obtained using 28 electrodes. The open diamonds are $(E_{1/2} - E°')_\Delta$ values computed from eq 9 using $k°$ and α values determined from the method of Bard and Mirkin (Table 1). The smooth lines correspond to theoretical predictions, eq 9, using $k°$ values of 1 (the estimated lower limit), 5 (the best fit based on $\Delta E_{1/4}$ and $\Delta E_{3/4}$ values), and 10 cm/s (the best fit based on experimental $E_{1/2}$ values). A value of $\alpha = 0.6$ was assumed in all calculations.

Values of $(E_{1/2} - E°')$ measured for the same 19 electrodes described above are listed in Table 1, using the subscript "expt" to indicate that they are experimental values, and plotted in Figure 7 as a function of r_{app}. The best fit of eq 10 to these data yields

(43) It is stated in ref 42 that kinetic analysis based on $\Delta E_{1/4} \leq 31$ mV and $\Delta E_{3/4} \leq 32$ mV for microdisk electrodes, and $\Delta E_{1/4} \leq 30.5$ mV and $\Delta E_{1/4} \leq 31$ mV for uniformly accessible electrodes, results in a large uncertainty in the calculated electron-transfer rate. Table 1 includes some data near these limits (corresponding to larger electrodes, $r_{app} > \sim 50$ nm) because the measurable shift in the half-wave potential indicated a real kinetic limitation. The use of small values of $\Delta E_{1/4}$ and $\Delta E_{3/4}$ appears to be justified, as $k°$ does not depend on the electrode size.

$k^\circ = 10.4 \pm 8.4$ cm/s, a value that is within error of that determined by analysis of $(E_{1/4} - E_{1/2})$ and $(E_{1/2} - E_{3/4})$ values.

The larger standard deviation in k° values determined from values of $(E_{1/2} - E^{\circ\prime})$ is due to the fact that this quantity is computed as a function of small difference in the $E_{1/2}$ values of the 25-μm-radius Pt electrode ($\approx E^{\circ\prime}$) and nanometer-size Pt electrodes. A small drift (a few millivolts) in the reference electrode potential between measurements, or small error in reading $E_{1/2}$, is propagated as a significant error in the computed value of k°. For example, the experimental value of $(E_{1/2} - E^{\circ\prime}) = 6.7$ mV for the 25.4-nm-radius electrode listed in Table 1 corresponds to a k° value of 11.5 cm/s. Assuming an error of ± 2 mV in $(E_{1/2} - E^{\circ\prime})$ corresponds to k° lying between 8.9 and 16 cm/s (note that the propagated error is asymmetric due to the nonlinear nature of eq 10). In contrast, the method of Mirkin and Bard relies on measurement of $(E_{1/4} - E_{1/2})$ and $(E_{1/2} - E_{3/4})$ from the same voltammogram, eliminating any error associated with the reference electrode potential. For this reason, the smaller rate constant obtained from $(E_{1/4} - E_{1/2})$ and $(E_{1/2} - E_{3/4})$ values is probably more reliable.

Figure 7 shows a comparison of the dependence of $(E_{1/2} - E^{\circ\prime})$ on r_{app} obtained directly from experiment (denoted with the subscript "expt") with $(E_{1/2} - E^{\circ\prime})$ values computed using eq 9 by employing values of k° determined by analysis of $(E_{1/4} - E_{1/2})$ and $(E_{1/2} - E_{3/4})$ values (denoted by the subscript "Δ"). This plot contains measurements from 28 electrodes, including the 19 listed in Table 1 in which both $(E_{1/2} - E^{\circ\prime})_{expt}$ and $(E_{1/2} - E^{\circ\prime})_\Delta$ were obtained. In addition to the data, theoretical curves are plotted for $k^\circ = 1$, 5, and 10 cm/s.

Several conclusions are apparent from visual inspection of Figure 7. First, despite the obviously large scatter in the data, essentially all data points lie well to the left-hand side of the theoretical line for $k^\circ = 1$ cm/s. Thus, we are confident that k° is significantly greater that 1 cm/s regardless of any argument concerning the electrode geometry. Second, the correlation between values of $(E_{1/2} - E^{\circ\prime})_{expt}$ and $(E_{1/2} - E^{\circ\prime})_\Delta$ is very weak. This finding suggests that the error in the kinetic analysis is not dominated by the nonideal electrode geometry but rather by random errors in measurement of $E_{1/4}$, $E_{1/2}$, and $E_{3/4}$, since any error associated with electrode geometry would propagate into $(E_{1/2} - E^{\circ\prime})_{expt}$ and $(E_{1/2} - E^{\circ\prime})_\Delta$ in the same direction. For instance, a recessed electrode geometry would result in negative deviations in *both* $(E_{1/2} - E^{\circ\prime})_{expt}$ and $(E_{1/2} - E^{\circ\prime})_\Delta$, not just one of these values. Third, while the data are clustered about the theoretical lines for $k^\circ = 5$ and 10 cm/s, it is readily apparent that the current precision of the measurement prevents being able to discern between these values.

The validity of the assumption that the $E_{1/2}$ value obtained at the 12.5-μm-radius Pt microdisk is a good approximation of $E^{\circ\prime}$, employed in the above analysis, can now be examined. This assumption is equivalent to assuming electron-transfer reversibility at the 12.5-μm-radius Pt and is valid if the rate of mass transfer is slow relative the rate of electron transfer; i.e., if $D/k^\circ r_{app} \ll 0.1$. Substituting experimental values of $k^\circ = 4.8$ cm/s, $D = 7.47 \times 10^{-6}$ cm^2/s, and $r_{app} = 12.5$ μm, yields $D/k^\circ r_{app} = 1.3 \times 10^{-3}$, yielding a negligibly small theoretical value for $(E_{1/2} - E^{\circ\prime})$, eq 10. Therefore, the assumption is clearly valid.

As a final comment, we note that the relative error in the standard rate constant reported by Mirkin et al. for the ferrocene/acetonitrile system ($k^\circ = 3.7 \pm 0.6$ cm/s) is much smaller ($\sim$16%) than reported here for the $TMAFc^+/H_2O$ system ($\sim$66%). The rate constant in the former case was measured by employing an SECM to position a 1.08-μm-radius Pt microdisk in close proximity to a larger Pt electrode. Positive feedback from the larger Pt electrode, at known microdisk-to-macrodisk separations, while recording the steady-state voltammogram at the microdisk, allows larger k° values to be measured than possible from the conventional voltammetric measurements described here. While this advantage is clear, evaluation of k° using a single Pt microdisk electrode would unlikely reveal sources of small errors in electrode geometry as well as nonperfect alignment of the microdisk and surrounding insulating shroud relative to the larger Pt surface. Thus, while the relative error in our measurement of k° is large, we believe that analysis of data from a large set of electrodes probably provides a realistic estimate of the error in kinetic measurements of fast electrode reactions using nanometer scale electrodes.

CONCLUSIONS

The method of Slevin et al. for preparing Pt electrodes with nanometer dimensions, based on electrophoretic coating of sharpened metal wires, appears to be capable of producing electrodes with geometries that can be described as an *approximate* hemisphere. However, high-resolution TEM suggests that the geometry of electrodes prepared at these length scales departs, to varying degrees, from the assumed ideal geometry. Theoretical models that account for the finite width of the insulating layer and subtle nonidealities in the geometry predict values of i_{lim} that are within the statistical error in the measurement.

Measurement of the true electrode area based on voltammetry of an adsorbed redox species appears to be promising for evaluating the area of nanoscale electrodes. In the preliminary measurements described here, we have measured electroactive areas as small as 10^{-10} cm^2. The lower limit of this measurement is currently determined in our hands by the capacitive charging of the electrode/polymer coating/solution interface and measurement noise, both issues where technological advances are possible and even likely. Thus, it appears reasonable that even smaller electroactive areas may be directly assessable to measurement soon.

A byproduct of our analysis of extremely small electrode areas is the demonstration of the ability to voltammetrically detect zeptomole quantities of an electroactive species. Ewing,[44–46] Wightman,[47] and others [48] have similarly reported amperometric and voltammetric measurements of zeptomole quantities of freely diffusing molecules following exocytic release from biological cells

(44) Chen, T. K.; Luo, G.; Ewing, A. G. *Anal. Chem.* **1994**, *66*, 3031−3035.
(45) Kozminski, K. D.; Gutman, D. A.; Davila, V.; Sulzer, D.; Ewing, A. G. *Anal. Chem.* **1998**, *70*, 3123−3130.
(46) Sombers, L. A.; Ewing, A. G. In *Electroanalytical Methods for Biological Materials*; Brajter-Toth, A., Chambers, J. Q., Eds.; Marcel Dekker: New York, 2002; pp 279−328.
(47) Hochstetler, S. E.; Puopolo, M.; Gustincich, S.; Raviola, E.; Wightman, R. M. *Anal. Chem.* **2000**, *72*, 489−496.
(48) An excellent review of amperometric and voltammetric detection during exocytosis is presented in ref 38.

using much larger electrodes (typically 5-μm radius) than employed in the current study. Thus, it appears that reducing the electrode dimensions to nanometer-length scales does not prevent electrochemical detection of such small quantities of molecules and may, in fact, be advantageous when high spatial resolution and ultrasensitive detection are simultaneously required.

Because of the current uncertainty in the electrode geometry, the use of just one or even a few electrodes of nanometer dimensions in kinetic studies of very fast heterogeneous rate constants is inadvisable, as a large over- or underestimation of k° is clearly possible. Analysis of the steady-state voltammetric quartile potentials of the 19 Pt nanoelectrodes yields a standard heterogeneous rate constant of $k^\circ = 4._8 \pm 3._2$ cm/s ($\alpha = 0.6_4 \pm 0.1_5$) for the $TMAFc^+/H_2O$ system. This value is similar to the value reported for the Fc/acetonitrile system (3.7 ± 0.6 cm/s), which suggests that differences in neither the solvent nor the methyltrimethylammonium pendant group of $TMAFc^+$ have a large effect on the rate of oxidation of the Fc moiety.

ACKNOWLEDGMENT

The authors thank Dr. Patrick Pinhero and Dr. Tedd Lister, Idaho National Engineering and Environmental Laboratory, for the SEM images and Mrs. Nancy Chandler, University of Utah Research Facilities, for her assistance with the TEM imaging. This research was supported by the Office of Naval Research.

SUPPORTING INFORMATION AVAILABLE

A schematic diagram showing the procedure for coating electrodes with Apiezon wax. This material is free of charge via the Internet at http://pubs.acs.org.

Received for review March 24, 2003. Accepted June 28, 2003.

AC0342931